

File G:

BRL MR 2594

BRL

AD 1021935

MEMORANDUM REPORT NO. 2594

EXPERIMENTAL PHOTODISSOCIATION AND/OR
PHOTODETACHMENT OF ATMOSPHERIC NEGATIVE
IONS: INITIAL RESULTS ON O_2^- AND CO_3^-

John A. Vanderhoff
Richard A. Beyer

February 1976

Approved for public release; distribution unlimited.

USA BALLISTIC RESEARCH LABORATORIES
ABERDEEN PROVING GROUND, MARYLAND

Destroy this report when it is no longer needed.
Do not return it to the originator.

Secondary distribution of this report by originating
or sponsoring activity is prohibited.

Additional copies of this report may be obtained
from the National Technical Information Service,
U.S. Department of Commerce, Springfield, Virginia
22151.

The findings in this report are not to be construed as
an official Department of the Army position, unless
so designated by other authorized documents.

UNCLASSIFIED

SECURITY CLASSIFICATION OF THIS PAGE (When Data Entered)

REPORT DOCUMENTATION PAGE		READ INSTRUCTIONS BEFORE COMPLETING FORM
1. REPORT NUMBER BRL MEMORANDUM REPORT NO. 2594	2. GOVT ACCESSION NO.	3. RECIPIENT'S CATALOG NUMBER
4. TITLE (and Subtitle) EXPERIMENTAL PHOTODISSOCIATION AND/OR PHOTODETACHMENT OF ATMOSPHERIC NEGATIVE IONS: INITIAL RESULTS ON O ₂ ⁻ and CO ₃ ⁻	5. TYPE OF REPORT & PERIOD COVERED Final	
	6. PERFORMING ORG. REPORT NUMBER	
7. AUTHOR(s) John A. Vanderhoff and Richard A. Beyer*	8. CONTRACT OR GRANT NUMBER(s)	
9. PERFORMING ORGANIZATION NAME AND ADDRESS US Army Ballistic Research Laboratories Aberdeen Proving Ground, MD 21005	10. PROGRAM ELEMENT, PROJECT, TASK AREA & WORK UNIT NUMBERS RDT&E IT161102B53A/15 DNA Subtask S99QAXHD010	
11. CONTROLLING OFFICE NAME AND ADDRESS US Army Materiel Development & Readiness Command 5001 Eisenhower Avenue Alexandria, VA 22333	12. REPORT DATE FEBRUARY 1976	
	13. NUMBER OF PAGES 30	
14. MONITORING AGENCY NAME & ADDRESS (if different from Controlling Office)	15. SECURITY CLASS. (of this report) UNCLASSIFIED	
	15a. DECLASSIFICATION/DOWNGRADING SCHEDULE	
16. DISTRIBUTION STATEMENT (of this Report) Approved for public release; distribution unlimited.		
17. DISTRIBUTION STATEMENT (of the abstract entered in Block 20, if different from Report)		
18. SUPPLEMENTARY NOTES *NRC/BRL Research Associate		
19. KEY WORDS (Continue on reverse side if necessary and identify by block number) Photodetachment Photodissociation Negative Ions Photon-Negative Ion Interaction Drift tube		
20. ABSTRACT (Continue on reverse side if necessary and identify by block number) A drift tube mass spectrometer apparatus with a laser photon source has been constructed to measure photodissociation and/or photodetachment cross sections of atmospheric negative ions. Values for the cross sections of the negative ions of molecular oxygen and carbon trioxide are in good agreement with published results. Most of the data obtained for the discrete energies available to the Kr ion laser represent new results. These results reinforce the existing evidence of substantial structure in the spectrum of the negative carbon trioxide ion photodestruction cross section.		

TABLE OF CONTENTS

	Page
LIST OF ILLUSTRATIONS.	5
I. INTRODUCTION	7
II. EXPERIMENTAL	7
III. ANALYSIS	11
IV. RESULTS.	12
V. EXPERIMENTAL ERROR	21
VI. CONCLUSION	22
REFERENCES	23
DISTRIBUTION LIST.	27

LIST OF ILLUSTRATIONS

<u>Figure</u>	<u>Page</u>
1. Schematic diagram of photodestruction experiment	8
2. (a) Negative ion mass spectra using $13.3 \text{ N/m}^2 \text{ O}_2$ gas with an $E/N = 10 \text{ Td. } (1 \times 10^{-20} \text{ V-m}^2)$.	
(b) Negative ion mass spectra using an O_2/CO_2 gas mixture ($5.33 \text{ N/m}^2 \text{ O}_2, 1.33 \text{ N/m}^2 \text{ CO}_2$) at an $E/N = 10 \text{ Td. } (1 \times 10^{-20} \text{ V-m}^2)$	13
3. Photodetachment cross section versus photon energy ($1 \text{ eV} = 1.602 \times 10^{-19} \text{ J}$) for O_2^- . The solid triangles are present results, the open triangles and solid line represent the data of Cosby et al. ⁸ , and the dashed line is an extrapolation of the data of Burch et al. ⁵	16
4. Photodestruction cross section versus photon energy for CO_3^- . The solid circles are present results, the open circles and half solid circles represent the data of Moseley et al. ^{22,23,29}	19

I. INTRODUCTION

Three-body attachment of electrons to atoms or molecules provides an abundance of negative ions in the D region of the atmosphere and below. A further sequence of reactions with neutral constituents results in the formation of a variety of negative ions. The more abundant species are O^- , O_2^- , O_3^- , O_4^- , CO_3^- , CO_4^- , NO_2^- , NO_3^- , and their hydrates.^{1*} These negative ions can be considered as a reservoir of electrons which can make a large contribution to the free electron concentration. Stimuli such as photons from sunlight or a nuclear burst may provide a trigger for this contribution. Several mechanisms can be responsible for freeing electrons from negative ions. Those mechanisms of interest here are: (1) direct detachment of the electron from the negative ion via photon absorption, and (2) a two step process the first of which is dissociation of the negative ion into a simpler negative ion plus neutral followed by detachment of the electron from the simpler negative ion.

Photodetachment measurements have been made for some atmospheric ions, i.e., O^- 2-4, O_2^- 4-9, OH^- 4,10-12, O_3^- 8,13-16, NO_2^- 4,17, NO_3^- 4, CO_3^- 4,18-20, $CO_3^- \cdot H_2O$ ¹⁸, and O_4^- 21. Recently photodestruction (photodissociation and/or photodetachment) measurements of ions of atmospheric interest have been pursued. Cross sections for O_2^- , O_3^- , O_4^- , CO_3^- , HCO_3^- , $CO_3^- \cdot H_2O$ and $HCO_3^- \cdot H_2O$ have been measured at selected wavelengths 8,22-24. Since experimental studies of atmospheric negative ions are still quite incomplete, we have initiated a laboratory investigation of such ions. This report contains the experimental details and the initial data obtained with the recently constructed experimental apparatus.

II. EXPERIMENTAL

The experimental apparatus consists of four major components: the negative ion source, the drift or thermalizing region, the mass spectrometer and ion detection electronics, and a laser. A schematic representation of the apparatus is shown in Figure 1. Initially,

* References are listed on page 23.

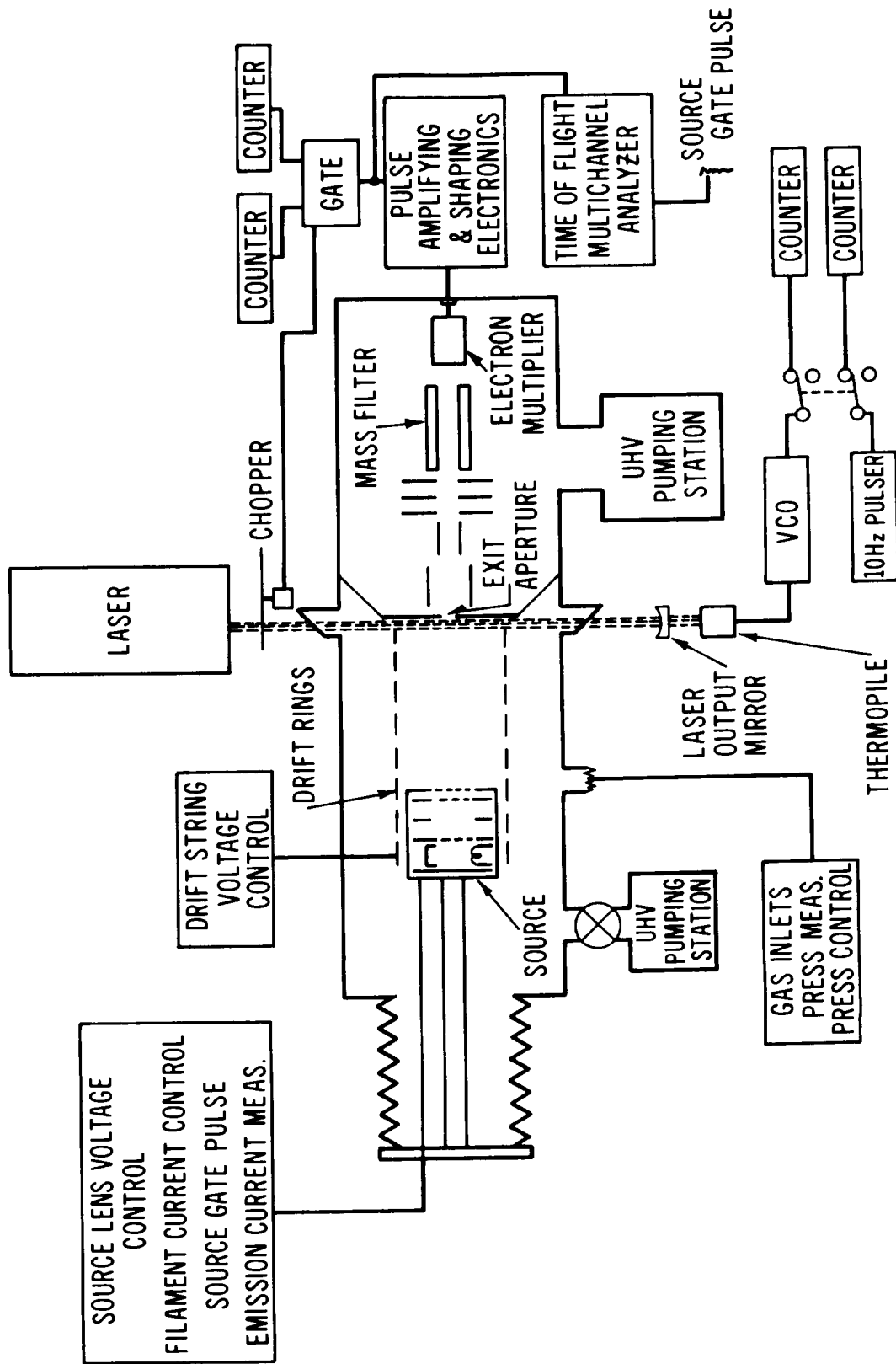


Figure 1. Schematic diagram of photodestruction experiment.

ions are formed in the source from which they are extracted into the drift region. Under the influence of a weak uniform electric field, the negative ions drift toward the exit aperture while making many low energy collisions with the neutral gas molecules. During this drift time the ions diffuse and possibly react with the neutral species. Just in front of the exit aperture the negative ion swarm is intersected by a chopped laser photon source. The ions which pass through the exit aperture are accelerated to a mass filter, detected by an electron multiplier and the counts are gated to one of two counters depending on chopper position.

Ions are formed in the source by dissociative attachment or three-body attachment of electrons to the neutral gas molecules. Electrons are emitted by a thoriated iridium filament and accelerated transverse to the drift direction to a collector where the current is monitored. A $\sim 7 \times 10^{-3} \text{ Wb/m}^2$ magnetic field in the direction of electron travel assists in confining the electrons to the filament-collector region and increases the number of electron-neutral collisions. Ions are extracted from this formation region through a 12 mm hole in the extractor plate. The remainder of the source consists of three lenses whose potentials may be adjusted to vary the ion residence time in the ion source region and thereby vary by up to an order of magnitude the relative concentrations of ions created by electron impact and those formed by subsequent ion-neutral reactions. The final lens is positioned in the midplane of a drift ring and is maintained at the potential of that ring. This arrangement provides a uniform drift field for the negative ions from the exit of the source to the sampling aperture. The last two lenses of the source can also be used to gate the ions. The resultant time arrival spectra can be used to extract ion mobilities and reaction rate coefficients.

The constant electric field drift region consists of eight evenly spaced stainless steel rings with 102 mm diameter. The 1.0 mm diameter exit aperture is centered in the midplane of the final, grounded drift ring. The negative potentials for the other seven drift rings are determined by an external voltage divider chain. The distance from the last source lens to the exit aperture can be varied from 2 to 125 mm by moving the source. The source is mounted to the main vacuum chamber by a welded diaphragm stainless steel bellows to allow this movement to be made under vacuum conditions.

Variation of the drift distance is used to adjust the relative concentrations of ions created or lost in ion-molecule reactions as well as allowing for relaxation of ions created in excited states. End effects²⁵ which may be important in mobility measurements can be eliminated by obtaining data at two or more drift distances. One may also obtain ion-molecule reaction rate constants by variation of the drift distance.²⁶

Ions passing through the exit aperture enter a region of low pressure, $\sim 10^{-3} \text{ N/m}^2$ as compared to $\sim 10 \text{ N/m}^2$ in the drift region. These ions are accelerated through collimating lens to a potential of ~ 30 volts before they enter the monopole mass filter which has approximately 1 amu resolution. A channeltron multiplier and associated pulse counting electronics detect, amplify, and record this incoming signal.

The photon source is a continuous duty ion laser with a beam diameter of approximately 1.4 mm. Both Ar and Kr laser tubes have been used. To maximize the photon intensity the output mirror of the laser was situated such that the interaction of the light beam with the negative ion swarm was inside the laser cavity. High quality quartz Brewster windows on the vacuum system and high reflectivity output mirrors were used to maximize intracavity light power. A thermopile was used to indicate the laser output power. To obtain the average power for the course of an experimental run the voltage output of the thermopile was converted to frequency and counted. This number along with a measurement of time for the run is used to calculate the average power. To convert this power into the actual intracavity power P_c the following relationship can be used

$$P_c(\lambda) = P_o(\lambda) \left[\frac{2 - T(\lambda)}{T(\lambda)} \right], \quad (1)$$

where $T(\lambda)$ is the transmission of the laser output mirror and P_o is the output power. The intracavity laser power for these experiments ranged from 1 to 50 watts. However, only relative power measurements were necessary to the reduction of the data presented here. The laser beam is modulated with a 50 percent duty cycle by an intracavity 93 Hz chopper. This chopper also controls the gating of the ion count pulses to one of two scalars alternately to give a measure of the ion count rate with light off and light on. As will be shown below, the ratio of these two numbers, along with the power and drift velocity measurements, can be used to calculate the photo-destruction cross section.

III. ANALYSIS

The resultant intensity of a negative ion species subjected to a photon flux is given by

$$I(\lambda) = I_0 e^{-B\sigma(\lambda)\phi(\lambda)t} \quad , \quad (2)$$

where I_0 is the initial negative ion intensity, $\sigma(\lambda)$ is the cross section for the photon-ion interaction, t is the average time an ion spends in the photon beam, $\phi(\lambda)$ is the photon flux, and B is a geometric term describing the overlap of the photon beam with the ion swarm which is sampled through the exit aperture.

The photodestruction cross section can be written as

$$\sigma(\lambda) = \frac{B}{t\phi(\lambda)} \ln \frac{N_0}{N(\lambda)} \quad , \quad (3)$$

where $N(\lambda)$ and N_0 are the counts detected at the particle multiplier with and without a flux of photons of wavelength λ , respectively. It is assumed that the negative ion intensity is proportional to these detected counts. For all data reported here the cross sections were measured relative to O^- . Absolute values for the photodetachment cross section of O^- at wavelengths of interest have been reported in the literature.²⁻⁴ By making a relative measurement, experimental conditions can be arranged such that the value of B is not required. However, we did perform initial checks by measuring the O^- photodetachment cross section.

Using six discrete lines of an Ar ion laser (514.5 nm, 501.7 nm, 496.5 nm, 488.0 nm, 476.5 nm, and 457.9 nm) the photodetachment cross section for O^- was measured. The values obtained were consistent with previous measurements in that they were constant to within 10 percent. The largest contribution to this fluctuation was likely the uncertainty in the laser output mirror transmission for these wavelengths. To obtain a cross section of $6.3 \times 10^{-18} \text{ cm}^2$ a value for B near unity was required. This value was anticipated since the photon beam diameter is 1.4 mm and the exit aperture is smaller (1.0 mm) and within 1 mm of the photon beam edge.

Normalization of the measured cross section to the O^- cross section eliminates uncertainties associated with B and the laser power. The photodestruction cross section of an ion A^- normalized to the O^- cross section can be written as

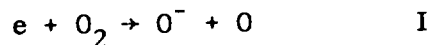
$$\sigma_{A^-}(\lambda) = \sigma_{O^-}(\lambda) \frac{\ln \left(\frac{N_O}{N(\lambda)} \right)_{A^-} \frac{P}{v_{A^-}}}{\ln \left(\frac{N_O}{N(\lambda)} \right)_{O^-} v_{O^-}}, \quad (4)$$

where $\frac{P}{v_{A^-}}$ is the ratio of laser powers $\left(\frac{P_{O^-}}{P_{A^-}} \right)_\lambda$ for the A^- and O^- cross section measurements. Since the laser beam is not altered during the acquisition of the O^- and A^- cross section data, the geometric term B does not change. The time an ion spends in the laser beam (2) has been replaced by the ion velocity. For the case where the ion makes a number of collisions while traversing the laser beam a drift velocity can be used for the ion velocity. Drift velocities were obtained from existing mobility data.²⁷⁻²⁹

Drift tube experiments usually report results as a function of the mean collision energy between the ions and the neutral gas. This energy is expressed by the ratio of the applied drift field to the neutral gas density, E/N. The units for E/N are $V m^2$ but are normally converted to Townsends ($1 \text{ Townsend (Td)} = 10^{-21} V m^2$). The cross section measurements reported here were made at an E/N of 10 Td. At this E/N the drift velocity for O^- is approximately an order of magnitude less than thermal velocity. With this weak field the negative molecular ions are thermalized while traversing the drift region.

IV. RESULTS

Photodestruction cross section measurements for O_2^- and CO_3^- were performed in O_2 and O_2/CO_2 mixtures, respectively. Figure 2a shows the negative ions formed in $13.3 N/m^2$ ultra high purity O_2 . Primary reactions for the formation of O^- and O_2^- are



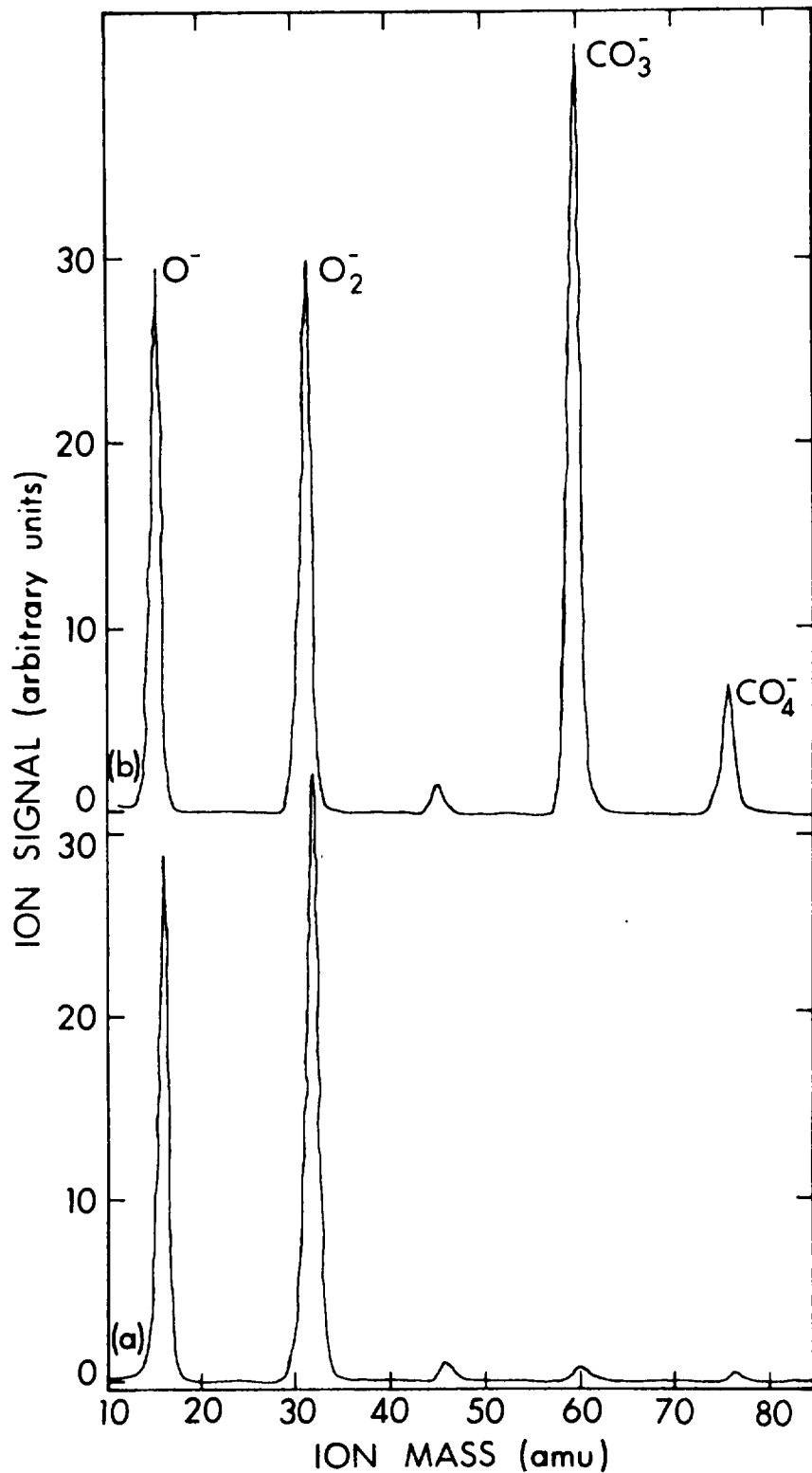
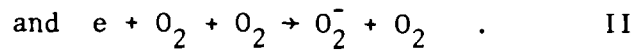


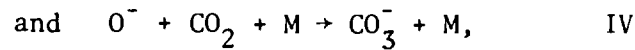
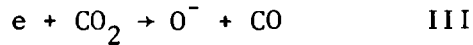
Figure 2. (a) Negative ion mass spectra using $13.3 \text{ N/m}^2 \text{ O}_2$ gas with an $E/N = 10 \text{ Td}$. ($1 \times 10^{-20} \text{ V}\cdot\text{m}^2$).
 (b) Negative ion mass spectra using an O_2/CO_2 gas mixture ($5.33 \text{ N/m}^2 \text{ O}_2$, $1.33 \text{ N/m}^2 \text{ CO}_2$) at an $E/N = 10 \text{ Td}$. ($1 \times 10^{-20} \text{ V}\cdot\text{m}^2$).



Residual amounts of CO_2 in the apparatus resulted in small quantities of CO_3^- and CO_4^- also being formed in this ion spectrum. These quantities of CO_3^- and CO_4^- could effect the photodetachment cross section measurements of O_2^- in the following way. Moseley et al.^{22,23} have found that most, if not all, of the photodestruction of CO_3^- is by breaking up into O^- and CO_2 . This provides a source term for O^- not accounted for. However, the photodestruction cross section for CO_3^- is more than a factor of three smaller than the O^- photodetachment cross section over the photon energy range studied here. Assuming no mass discrimination the concentration of CO_3^- is about 3 percent that of O^- . If we now assume maximum efficiency for the collection of the photofragment O^- then this would be a 1 percent effect on the results. Since the dissociation energy of CO_4^- into O_2^- and CO_2 is 0.8 eV¹ (1eV = 1.602×10^{-19} J), it can contribute to the O_2^- concentration during laser on conditions. Our preliminary measurements of the CO_4^- photodestruction cross section at 676.4 nm, 647.1 nm, and 514.5 nm indicate its value is substantially less than the photodetachment cross section of O_2^- . Moseley has measured the photodestruction cross section for CO_4^- in the wavelength region from 660 to 515.5 nm and finds values less than $2 \times 10^{-19} \text{ cm}^2$. This cross section together with the quantity of CO_4^- present in the ion spectrum make possible errors from this effect less than 0.3 percent.

A negative ion impurity at an m/e of 46 is present in the ion spectrum. The identity of this ion is most likely NO_2^- since some experimental testing was carried out using nitric oxide gas in the system. The photodestruction cross section for this ion was measured to be negligible with respect to an introduction of error in the present results.

Figure 2b shows the negative ions formed in a carbon dioxide and oxygen gas mixture. In addition to producing negative ions from reactions I and II O^- and CO_3^- can be formed by the reactions



where M is the third body. The ratio of CO_4^- to O_2^- produced in this case is about 25 percent and from previous arguments the maximum uncertainty caused from the CO_4^- is less than 5 percent.

From the results of other investigators,⁴⁻⁹ as well as the dissociation energy of O_2^- as 4.08 eV^1 , the photodestruction of O_2^- over the photon energy range of this study can be considered as composed entirely of photodetachment. The present photodetachment cross section measurements for O_2^- at selected wavelengths are displayed as solid triangles in Figure 3. These values together with the statistical uncertainties resulting from counting are listed in Table 1. Ar and Kr ion lasers with prism wavelength selectors were used to obtain the discrete photon energies with approximately $1 \times 10^{-5} \text{ eV}$ resolution. Low field reduced mobility values for O^- and O_2^- drifting in O_2 measured by Snuggs et al.²⁷ have been used to calculate the required drift velocities for O^- and O_2^- . These mobility values are 3.20 for O^- and 2.16 for O_2^- .

Photodetachment values for O_2^- using an Ar ion laser have been reported by Cosby et al.⁸ and are represented by open triangles on Figure 3. More recently this group used an Ar laser to pump a tunable dye laser and thus measured the O_2^- photodetachment cross section continuously from 670 to 565 nm with a photon energy width of approximately $1 \times 10^{-4} \text{ eV}$. These measurements were averaged to yield the solid line in Figure 3. Burch et al. and Warneck using a beam technique with a glow discharge ion source have also measured the O_2^- photodetachment cross section. The dashed line represents an extrapolation of the data of Burch et al. from 1.82 to 2.72 eV. These data have a photon energy resolution of about 0.2 eV. The data of Warneck with a 0.07 eV photon energy resolution are not plotted but follow closely the data of Burch et al.

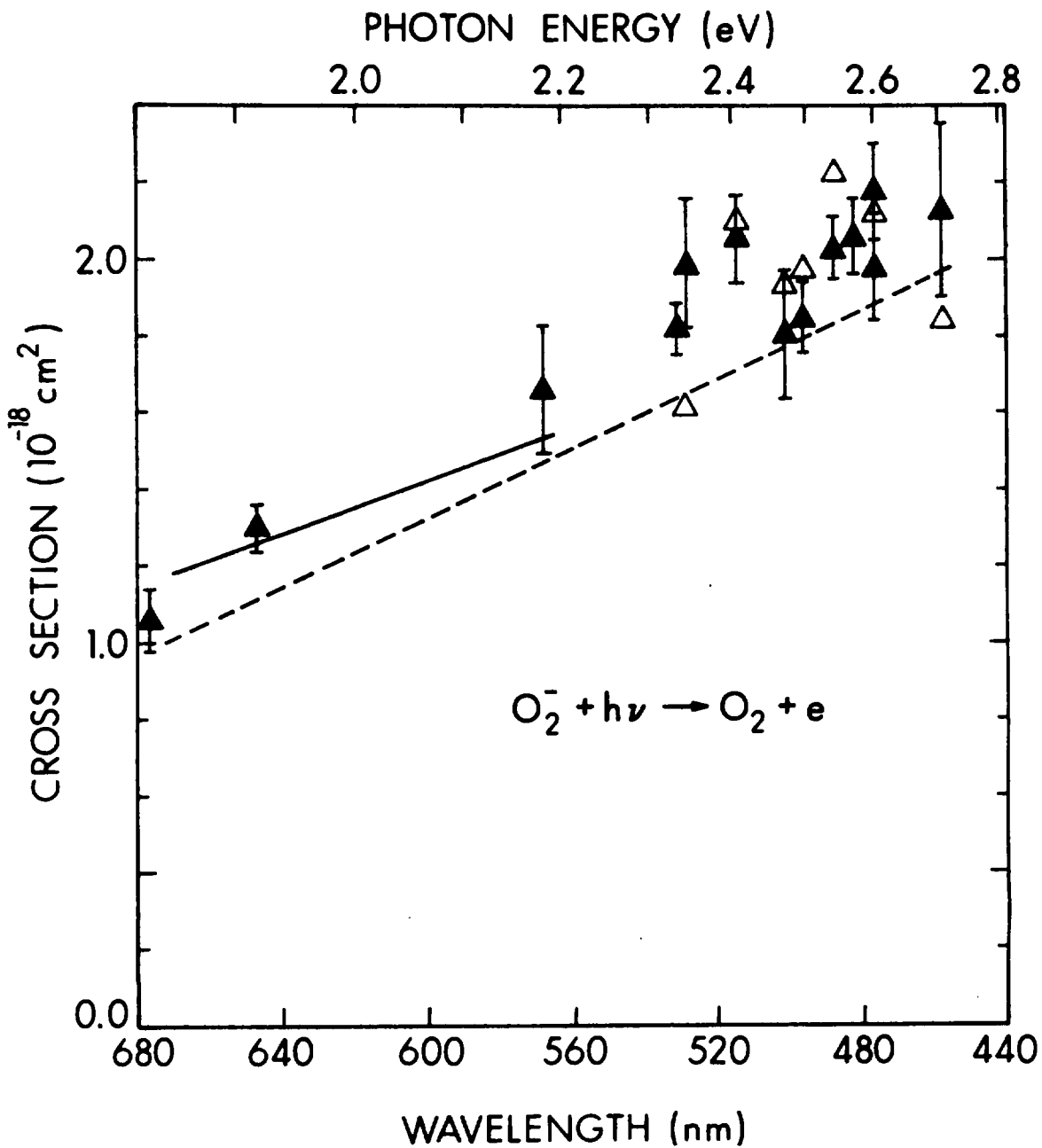


Figure 3. Photodetachment cross section versus photon energy ($1 \text{ eV} = 1.602 \times 10^{-19} \text{ J}$) for O_2^- . The solid triangles are present results, the open triangles and solid line represent the data of Cosby et al.⁸, and the dashed line is an extrapolation of the data of Burch et al.⁵

TABLE I. Photodestruction Cross Section Values for O_2^- and CO_3^- .

Negative Ion	Photon Wavelength (nm)	Photon Energy (eV)	Photodestruction Cross Section (10^{-18} cm^2)	Statistical Uncertainty (10^{-18} cm^2)
O_2^-	676.4	1.833	1.06	± 0.08
	647.1	1.916	1.30	0.06
	568.2	2.182	1.66	0.17
	530.9	2.335	1.82	0.07
	528.7	2.345	1.99	0.17
	514.5	2.410	2.06	0.12
	501.7	2.471	1.80	0.17
	496.5	2.497	1.85	0.10
	488.0	2.540	2.03	0.08
	482.5	2.569	2.06	0.10
	476.5	2.602	2.18	0.13
	476.2	2.603	1.98	0.14
	457.9	2.707	2.13	0.23
CO_3^-	676.4	1.833	0.09	0.04
	647.1	1.916	0.98	0.07
	568.2	2.182	1.34	0.36
	530.9	2.335	1.01	0.12
	514.5	2.410	0.75	0.09
	501.7	2.471	0.80	0.21
	496.5	2.497	0.53	0.10
	488.0	2.540	0.45	0.06
	482.5	2.569	0.49	0.13
	476.5	2.602	0.77	0.12
	476.2	2.603	0.93	0.19
	457.9	2.707	0.88	0.32

Larger photodetachment values for O_2^- (not shown) have been reported by Burt⁷ who conducted an experiment in O_2 with pressures ranging from 66.6 to 359.6 N/m². These results have been questioned by Cosby et al. as possibly being affected by the photodissociation of O_3^- .

The general agreement for the photodetachment measurements of O_2^- is quite good. The higher photon energy resolution results in the 2.35 to 2.71 eV energy range indicate possible structure in the O_2^- photodetachment cross section; however, a detailed investigation over this energy range is required to determine if structure exists as opposed to a smoothly increasing cross section.

Photodestruction cross section measurements for CO_3^- were conducted in O_2/CO_2 gas mixtures to eliminate the need to use O^- for normalization since CO_3^- photodissociates to form O^- . With the O_2/CO_2 mixtures sufficient quantities of O_2^- are created for use in normalization. The total gas pressure employed was 6.66 N/m² and the amount of CO_2 in the mixture ranged from 20 to 50 percent. The CO_3^- photodestruction data obtained is shown as solid circles in Figure 4. The error bars represent only the statistical uncertainty for the CO_3^- counting. These photodestruction values at selected wavelengths are listed in Table I. Along with these values are the statistical uncertainty resulting from the counting for both CO_3^- and the O_2^- used for normalization.

To obtain the required drift velocities for O_2^- and CO_3^- drifting in an O_2/CO_2 gas mixture the following procedure was used. Low field reduced mobilities for O^- and CO_3^- drifting in CO_2 have been measured by Moseley²⁹ as $1.92 \times 10^{-4} \text{ m}^2/\text{V-sec}$ and $1.34 \times 10^{-4} \text{ m}^2/\text{V-sec}$, respectively. Snuggs et al.²⁷ have measured the reduced mobility of CO_3^- in O_2 as $2.50 \times 10^{-4} \text{ m}^2/\text{V-sec}$. However, we have not found any published values for the mobility of O_2^- in CO_2 . This drift velocity was therefore computed by substitution into an equation given by

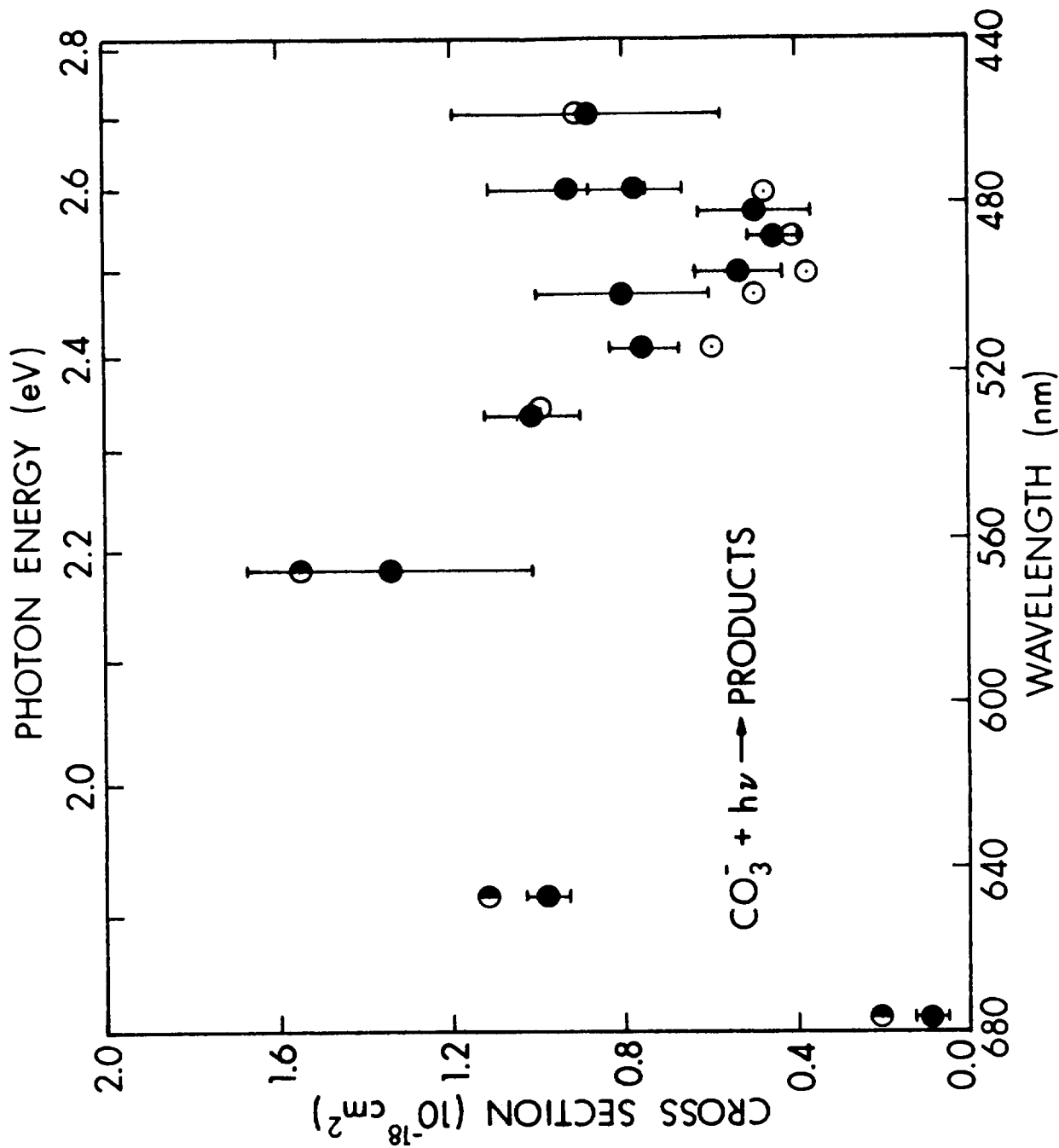


Figure 4. Photodestruction cross section versus photon energy for CO_3^- . The solid circles are present results, the open circles and half solid circles represent the data of Moseley et al.^{22,23,29}

McDaniel and Mason.²⁸ This equation for the low field drift velocity of an ion in a neutral gas is

$$v_d(0) = \frac{\xi}{3^{1/2}} \left(\frac{1}{m} + \frac{1}{M} \right) \frac{e}{(kT)^{1/2}} Q \left(\frac{E}{N} \right) \quad (5)$$

where m and M are the masses of the ion and neutral respectively. Q is the collision cross section and ξ is a factor of order unity. Equation 5 can be written for different species (1 & 2), assuming $\xi_1 = \xi_2$ and $Q_1 = Q_2$ then

$$\frac{v_{d1}(0)}{v_{d2}(0)} = \frac{K_1(0)}{K_2(0)} = \frac{\left(\frac{1}{m_1} + \frac{1}{M_1} \right)^{1/2}}{\left(\frac{1}{m_2} + \frac{1}{M_2} \right)^{1/2}}, \quad (6)$$

where $K_1(0)$ and $K_2(0)$ are the low field reduced mobilities of species 1 and 2, respectively. By substitution of the mobility for O^- in CO_2 into Equation 6 we compute the mobility of O_2^- in CO_2 to be $1.53 \times 10^{-4} \text{ m}^2/\text{V-sec}$.

These mobility values together with the fractional composition of the gas mixture substituted into Blanc's Law,

$$\frac{1}{K_{12}(0)} = \frac{x_1}{K_1(0)} + \frac{x_2}{K_2(0)}, \quad (7)$$

give the required low field ion mobilities for the gas mixture. Here $K_{12}(0)$ is the low field mobility of an ion species in a gas mixture of fractional composition $x_1 + x_2$.

Photodestruction cross section values for CO_3^- reported by Moseley et al.^{22,23,29} are also plotted on Figure 4. The open circles represent their data using an Ar ion laser and the half solid circles represent data taken using an Ar ion laser pumped tunable dye laser. Burt has reported larger photodetachment cross sections for CO_3^- in the photon energy range studied here; however,

the interpretation of his cross sections as being due to photodetachment has been questioned by Ferguson et al.¹⁹ whose calculations indicate the electron affinity of $\text{CO}_3^- \geq 2.9$ eV. As mentioned earlier Moseley et al.^{22,23} report that most, if not all the photodestruction in this energy range is due to photodissociation. Under conditions where CO_3^- was the dominant ion, we observed photoproduction of O^- at 514.5 nm.

The agreement between the two sets of data shown in Figure 4 is good and suggests detailed structure may be present. Cosby et al.²⁴ have used a tunable dye laser to obtain an abundance of structure over the range 640 to 565 nm. They interpret their spectra as resulting from vibrational structure of a bound, predissociating state.

V. EXPERIMENTAL ERROR

In this section the experimental uncertainties will be discussed and summed to give an estimate of the overall accuracy of the data obtained.

The experimental errors can be split into two categories; relative error and absolute error. The relative error can be thought of as that error associated with the experimental apparatus. That is, given that the apparatus measures one data point correctly, the relative error is the error associated with the other data points measured with the same apparatus. Contributions to the relative error consist of (from Equation 4) statistical counting errors, ion velocity ratio errors, and laser power ratio error.

The statistical error taken for each counting measurement is \sqrt{N} . By combining these counting errors as a root mean square, the total counting error for each data point is obtained. Since this error is usually different for each data point, it is displayed as error bars on Figures 3 and 4. The ion velocities were not measured with the experimental apparatus, and therefore this error is more appropriately discussed as absolute error. However, errors and/or changes in the drift field voltage, temperature, and gas pressure can influence the ion velocities. We estimate the error in the ratio of the ion velocities due to these contributions to be ± 4 percent.

The laser power ratio measurement P due to the frequency range used for the voltage to frequency conversion is ± 3 percent. The root mean square of these two contributions is ± 5 percent which when added to the counting error represents a measure of the relative error.

The absolute error consists of the error associated with the absolute measurement of the O_2^- photodetachment cross section (± 10 percent)^{2,3} and the error associated with the computation of the drift velocities (± 4 percent)²⁷. The root mean square of these contributions yields an absolute error of ± 13 percent.

The above quoted errors are only directly applicable to the O_2^- results. The CO_3^- data reduction involved a two-step process. First the O_2^- photodetachment cross sections were measured and these results were necessary for the CO_3^- normalization. Consequently an additional relative error in counting exists. The root mean square of these counting uncertainty contributions for CO_3^- is reflected in Table 1. Additionally it was necessary to calculate the mobility of O_2^- in CO_2 from Equation 6. This could make the error associated with the drift velocities used for the CO_3^- photodestruction data slightly larger; however, for present purposes we assume the ± 4 percent is a generous estimate.

VI. CONCLUSION

Including possible errors in the present data these results reinforce the validity of the photodetachment cross section measurements for O_2^- and the photodestruction cross section measurements for CO_3^- made by Moseley et al.²² In addition the present Kr ion laser lines extend the photon energy range for photodestruction of these ions at discrete wavelengths.

REFERENCES

1. A. V. Phelps, "Electron Attachment and Detachment Processes", Chapter 17, DNA Reaction Rate Handbook, 2nd Edition, DNA 1948H (March 1972).
2. L. M. Branscomb, D. S. Burch, S. J. Smith, and S. Geltman, "Photodetachment Cross Section and the Electron Affinity of Atomic Oxygen," Phys. Rev. 111, 504, 1958.
3. L. M. Branscomb, S. J. Smith, and G. Tisone, "Oxygen Metastable Atom Production Through Photodetachment," J. Chem. Phys. 43, 2906, 1965.
4. P. Warneck, "Laboratory Measurements of Photodetachment Cross Sections of Selected Negative Ions," GCA Technical Report 69-13-N, GCA Corporation, Bedford, MA 1969).
5. D. S. Burch, S. J. Smith, and L. M. Branscomb, "Photodetachment of O_2^- ," Phys. Rev. 112, 171, 1958.
6. S. B. Woo, L. M. Branscomb, and E. C. Beaty, "Sunlight Photodetachment Rate of Ground State O_2^- ," J. Geophys. Res. 76, 2933, 1969.
7. J. A. Burt, "Experimental Measurement of the O_2^- Photodetachment Cross Section," Can. J. Phys. 50, 2410, 1972.
8. P. C. Cosby, R. A. Bennett, J. R. Peterson, and J. T. Moseley, "Photodissociation and Photodetachment of Molecular Negative Ions II. Ions Formed in Oxygen," J. Chem. Phys. 63, 1612, 1975 and BRL Contract Report No. 238 (USA BRL, Aberdeen Proving Ground, MD. 1975). AD# A012277.
9. R. J. Celotta, R. A. Bennett, J. L. Hall, M. W. Siegel, and J. Levine, "Molecular Photodetachment Spectrometry II, The Electron Affinity of O_2 and the Structure of O_2^- ," Phys. Rev. A 6, 631, 1972.
10. L. M. Branscomb, "Photodetachment Cross Section, Electron Affinity, and Structure of the Negative Hydroxyl Ion," Phys. Rev. 148, 11, 1966.
11. R. J. Celotta, R. A. Bennett, and J. L. Hall, "Laser Photodetachment Determination of the Electron Affinities of OH, NH_2 , NH, SO_2 , and S_2 ," J. Chem. Phys. 60, 1740, 1974.
12. H. Hotop, T. A. Patterson, and W. C. Lineberger, "High Resolution Photodetachment Study of OH^- and OD^- in the Threshold Region, 7000-6450Å" J. Chem. Phys. 60, 1806, 1974.

13. R. Byerly, Jr, and E. C. Beaty, "Sunlight Photodetachment of O_3^- ," J. Geophys. Res. 76, 4596, 1971.
14. S. F. Wong, T. V. Vorburger, and S. B. Woo, "Photodetachment of O_3^- in a Drift Tube," Phys. Rev. A 5, 2598, 1972.
15. J. A. Burt, "Measurement of the Cross Section for Photodetachment of O_3^- ," Ann. Geophys. 28, 607, 1972.
16. G. Sinnott and E. C. Beaty, Seventh International Conference on the Physics of Electronics and Atomic Collisions: Abstracts of Papers (North Holland Publishing, Amsterdam, 1971) p. 176.
17. E. Herbst, T. A. Patterson, and W. C. Lineberger, "Laser Photodetachment of NO_2^- ," J. Chem. Phys. 61, 1300, 1974.
18. J. A. Burt, "Photodetachment Cross Section for CO_3^- and Its First Hydrate," J. Chem. Phys. 57, 4649, 1972.
19. E. E. Ferguson, F. C. Fehsenfeld, and A. V. Phelps, "Comment on Photodetachment Cross Sections for CO_3^- and Its First Hydrate," J. Chem. Phys. 59, 1565, 1973.
20. J. A. Burt, "Reply to Comments on Photodetachment Cross Section for CO_3^- and Its First Hydrate," J. Chem. Phys. 59, 1567, 1973.
21. J. A. Burt, "Measurement of the Photodetachment Cross Section for O_4^- at High Pressure," J. Geophys. Res. 77, 6280, 1972.
22. J. T. Moseley, R. A. Bennett, and J. R. Peterson, "Photodissociation of CO_3^- ," Chem. Phys. Letters 26, 288, 1974 and BRL Contract Report No. 144, (USABRL, Aberdeen Proving Ground, MD. 1974). AD# 777512.
23. J. T. Moseley, P. C. Cosby, R. A. Bennett, and J. R. Peterson, "Photodissociation and Photodetachment of Molecular Negative Ions I. Ions Formed in CO_2/H_2O Mixtures," J. Chem. Phys. 62, 4826, 1975 and "BRL Contract Report No. 236 (USABRL, Aberdeen Proving Ground, MD. 1975). AD# A012276.
24. P. C. Cosby and J. T. Moseley, "Photodissociation Spectrum of CO_3^- : Evidence for a Bound Excited State," Phys. Rev. Letters 34, 1603, 1975.

25. D. L. Albritton, T. M. Miller, D. W. Martin, and E. W. McDaniel, "Mobilities of Mass Identified H_3^+ and H^+ Ions in Hydrogen," Phys. Rev. 171, 94, 1968.
26. J. T. Moseley, R. M. Snuggs, D. W. Martin, and E. W. McDaniel, "Mobilities, Diffusion Coefficients, and Reaction Rates of Mass Identified Nitrogen Ions in Nitrogen," Phys. Rev. 178, 240, 1969.
27. R. M. Snuggs, D. J. Volz, J. H. Schummers, D. W. Martin, and E. W. McDaniel, "Ion Molecule Reactions between O^- and O_2 at Thermal Energies and Above," Phys. Rev. A 3, 477, 1971.
28. E. W. McDaniel and E. A. Mason, The Mobility and Diffusion of Ions in Gases (John Wiley and Sons, New York, 1973).
29. J. T. Moseley, private communication.

DISTRIBUTION LIST

<u>No. of Copies</u>	<u>Organization</u>	<u>No. of Copies</u>	<u>Organization</u>
12	Commander Defense Documentation Center ATTN: DDC-TCA Cameron Station Alexandria, VA 22314	1	Director Defense Communications Agency ATTN: Code 340, Mr. W. Dix Washington, DC 20305
1	Director Institute for Defense Analysis ATTN: Dr. E. Bauer 400 Army-Navy Drive Arlington, VA 22202	1	Director Defense Intelligence Agency Washington, DC 20301
1	Director Defense Advanced Research Projects Agency 1400 Wilson Boulevard Arlington, VA 22209	1	Commander US Army Materiel Development and Readiness Command ATTN: DRCDMA-ST 5001 Eisenhower Avenue Alexandria, VA 22333
2	Director of Defense Research and Engineering ATTN: (AD/EPS), LTC W. A. Whitaker COL A. J. Kaehn Washington, DC 20305	1	Commander US Army Materiel Development and Readiness Command ATTN: DRCDE-WN, Mr. J. Corrigan 5001 Eisenhower Avenue Alexandria, VA 22333
4	Director Defense Nuclear Agency ATTN: STAP (APTL) STRA (RAAE), Dr. C. Blank Dr. H. Fitz, Jr. DDST, Mr. W. Berning Washington, DC 20305	1	Commander US Army Aviation Systems Command ATTN: DRSAV-E 12th and Spruce Streets St. Louis, MO 63166
2	DASIAC/DOD Nuclear Information and Analysis Center General Electric Company-TEMPO ATTN: Mr. A. Feryok Mr. W. Knapp 816 State Street P.O. Drawer QQ Santa Barbara, CA 93102	1	Director US Army Air Mobility Research and Development Laboratory Ames Research Center Moffett Field, CA 94035
		1	Commander US Army Electronics Command ATTN: DRSEL-RD Fort Monmouth, NJ 07703

DISTRIBUTION LIST

<u>No. of Copies</u>	<u>Organization</u>	<u>No. of Copies</u>	<u>Organization</u>
1	Commander/Director Atmospheric Sciences Laboratory US Army Electronics Command ATTN: Mr. H. Ballard Mr. H. Rachele White Sands Missile Range NM 88002	1	Commander US Army Nuclear Agency ATTN: Mr. J. Berberet Fort Bliss, TX 79916
1	Commander US Army Missile Command ATTN: DRSMI-R Redstone Arsenal, AL 35809	1	Commander US Army Research Office ATTN: Dr. A. Dodd P.O. Box 12211 Research Triangle Park NC 27709
1	Commander US Army Tank Automotive Logistics Command ATTN: DRSTA-RHFL Warren, MI 48090	2	Commander US Army BMD Systems Command ATTN: SSC-HS, Mr. H. Porter SSC-TET, Mr. E. Carr P.O. Box 1500 Huntsville, AL 35807
2	Commander US Army Mobility Equipment Research & Development Command ATTN: Tech Docu Cen, Bldg 315 DRSME-RZT Fort Belvoir, VA 22060	1	Director US Army Ballistic Missile Defense Program Office ATTN: Dr. A. Gold Mr. J. Davidson Mr. J. Shea 1320 Wilson Boulevard Arlington, VA 22209
1	Commander US Army Armament Command Rock Island, IL 61202	1	HQDA (DAEN-RDM/Dr. de Percin) Washington, DC 20314
2	Commander US Army Harry Diamond Labs ATTN: DRXDO-TI DRXDO-NP, Mr. F. Wimenitz 2800 Powder Mill Road Adelphi, MD 20783	1	Chief of Naval Research ATTN: Code 418, Dr. J. Dardis Department of the Navy Washington, DC 20360
1	Commander US Army TRADOC Systems Analysis Activity ATTN: ATAA-SA White Sands Missile Range NM 88002	1	Commander US Naval Surface Weapons Center ATTN: Dr. L. Rutland Silver Spring, MD 20910
		1	Commander US Naval Electronics Laboratory ATTN: Mr. W. Moler San Diego, CA 92152

DISTRIBUTION LIST

<u>No. of</u> <u>Copies</u>	<u>Organization</u>	<u>No. of</u> <u>Copies</u>	<u>Organization</u>
3	Director US Naval Research Laboratory ATTN: Dr. W. Ali Code 7700, Mr. J. Brown Code 2020, Tech Lib Washington, DC 20330	1	General Electric Company Valley Forge Space Technology Center ATTN: Dr. M. Bortner P.O. Box 8555 Philadelphia, PA 19101
3	HQ USAF (AFNIN; AFRD; AFRDQ) Washington, DC 20330	1	Mission Research Corporation ATTN: Dr. M. Schiebe 812 Anacapa Street, Studio 5 Santa Barbara, CA 93101
1	AFOSR (SREP) 1400 Wilson Boulevard Arlington, VA 22209	1	R&D Associates ATTN: Dr. F. Gilmore P.O. Box 9695 Marine del Rey, CA 90291
2	AFSC (DLCAW, LTC R. Linkous; SCS) Andrews AFB Washington, DC 20331	2	Sandia Laboratories ATTN: Org 3141, Tech Lib Org 100, F. Hudson P.O. Box 5800 Albuquerque, NM 87115
1	AFWL (SYT) Kirtland AFB, NM 87115		
1	Director National Oceanic and Atmospheric Administration ATTN: Dr. E. Ferguson US Department of Commerce Boulder, CO 80302	1	Pennsylvania State University Ionospheric Research Laboratory ATTN: Dr. L. C. Hale University Park, PA 16802
1	Director Brookhaven National Laboratory ATTN: Docu Sec 25 Brookhaven Avenue Upton, NY 11973	3	Stanford Research Institute ATTN: Dr. J. Peterson Dr. J. Moseley Dr. P. Cosby 333 Ravenswood Avenue Menlo Park, CA 94025
2	Director Los Alamos Scientific Laboratory ATTN: Lib Dr. W. Maier (Gp J-10) P.O. Box 1663 Los Alamos, NM 87544	1	State University of New York Department of Atmospheric Sciences ATTN: Dr. V. Mohnen Albany, NY 12203
1	Bell Telephone Laboratories, Inc. Technical Report Service ATTN: Tech Rpts Specialist WH 5E-227 Whippany, NJ 07981	2	University of Colorado Joint Institute for Laboratory Astrophysics ATTN: Dr. W. C. Lineberger Dr. A. V. Phelps Boulder, CO 80304

DISTRIBUTION LIST

<u>No. of Copies</u>	<u>Organization</u>
1	University of Denver Denver Research Institute ATTN: Dr. R. Amme P.O. Box 10127 Denver, CO 82010
1	University of Illinois Electrical Engineering Department Aeronomy Laboratory ATTN: Prof. C. Sechrist Urbana, IL 61801
1	University of Minnesota, Morris Division of Science and Mathematics ATTN: Dr. M. N. Hirsh Morris, MN 56267
1	University of Pittsburg Cathedral of Learning ATTN: Dr. M. A. Biondi 400 Bellefield Avenue Pittsburg, PA 15213
1	University of Texas at El Paso Physics Department ATTN: J. Collins El Paso, TX 79902

Aberdeen Proving Ground

Marine Corps Ln Ofc
Dir, USAMSAA